AD-A192 184 ENVIRONMENTAL INTEGRITY OF COATING/METAL INTERFACE(U) 1/1
ROCKWELL INTERNATIONAL THOUSAND OAKS CA SCIENCE CENTER
M KENDIG ET AL JAN 88 SC5588 APR N00014-87-C-0075
UNCLASSIFIED F/G 7/6 NL

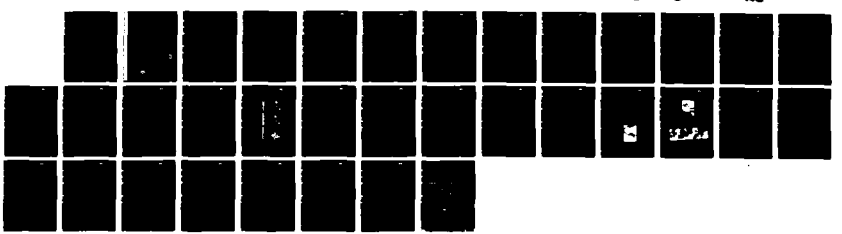

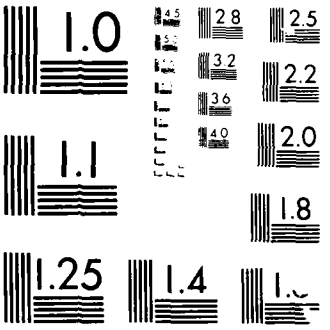

SC5508.APR

Copy No. 5

ENVIRONMENTAL INTEGRITY OF COATING/METAL INTERFACE

ANNUAL PROGRESS REPORT NO. 1 FOR THE PERIOD February 1, 1987 through January 31, 1988

CONTRACT NO. N00014-87-C-0075

Prepared for

Scientific Officer
Metallic Materials Division, Code 1131M
Office of Naval Research
800 North Quincy Street
Arlington, VA 22217-5000

Prepared by

M. Kendig, R. Addison and
S. Jeanjaquet

JANUARY 1988

Rockwell International
Science Center

UNCLASSIFIED

SECURITY CLASSIFICATION OF THIS PAGE

AD-A192 184

REPORT DOCUMENTATION PAGE

FORM APPROVED
OMB No. 0704-0188

1a REPORT SECURITY CLASSIFICATION **UNCLASSIFIED**	1b RESTRICTIVE MARKINGS
2a SECURITY CLASSIFICATION AUTHORITY	3 DISTRIBUTION/AVAILABILITY OF REPORT **Approved for public release; distribution unlimited**
2b CLASSIFICATION/DOWNGRADING SCHEDULE	
4 PERFORMING ORGANIZATION REPORT NUMBER(S) **SC5508.APR**	5 MONITORING ORGANIZATION REPORT NUMBER(S)
6a NAME OF PERFORMING ORGANIZATION **ROCKWELL INTERNATIONAL Science Center** 6b OFFICE SYMBOL (If Applicable)	7a NAME OF MONITORING ORGANIZATION
6c ADDRESS (City, State, and ZIP Code) **1049 Camino Dos Rios Thousand Oaks, CA 91360**	7b ADDRESS (City, State, and ZIP Code)
8a NAME OF FUNDING/SPONSORING ORGANIZATION **Office of Naval Research Metallic Materials Division, Code 1131M** 8b OFFICE SYMBOL (If Applicable)	9 PROCUREMENT INSTRUMENT IDENTIFICATION NUMBER **CONTRACT NO. N00014-87-C-0075**
8c ADDRESS (City, State, and ZIP Code) **800 North Quincy Street Arlington, VA 22217-5000**	10 SOURCE OF FUNDING NOS PROGRAM ELEMENT NO / PROJECT NO / TASK NO / WORK UNIT ACCESSION NO

11 TITLE (Include Security Classification)

ENVIRONMENTAL INTEGRITY OF COATING/METAL INTERFACE

12 PERSONAL AUTHOR(S)

M. Kendig, R. Addison and S. Jeanjaquet

13a TYPE OF REPORT	13b TIME COVERED	14 DATE OF REPORT (Year, Month, Day)	15 PAGE COUNT
Annual Progress Report No. 1	FROM **02/01/87** TO **01/31/88**	**1988, JANUARY**	**32**

16 SUPPLEMENTARY NOTATION

17 COSATI CODES			18 SUBJECT TERMS (Continue on reverse if necessary and identify by block number)
FIELD	GROUP	SUB-GROUP	**Organic coating, corrosion, cathodic disbonding, acoustic microscopy, polynbutadiene, adhesion, carbon steel**

19 ABSTRACT (Continue on reverse if necessary and identify by block number)

Corrosion of polymer coated steel in neutral media entails the initiation of anodic dissolution of the metal at defects in the coating with the cathodic reduction of oxygen at the adjacent interface. The cathodic reduction of oxygen produces a buildup of NaOH at the interface which enhances adhesion loss which leads to the propagation of corrosion. In-situ acoustic microscopy of a coating undergoing cathodic disbonding at constant potential has allowed evaluation of both the kinetics and microscopic structure of the disbond front with detail not previously attained. Disbonding of a hydroxy-terminated polybutadiene coating from polished and degreased steel in 0.5 M NaCl has been examined in-situ as a function of applied potential. The results show that potentials more negative than −550 mV vs Ag/AgCl accelerate disbonding by the formation of a weak fluid boundary layer at the coating/metal interface just ahead of electroosmotically produced ~50 μm blisters. Concentration of NaOH in the microblister weakens the polymer metal interface while the osmotic pressure in the microblisters provides the mechanical force necessary to rupture the coating/metal bond.

20 DISTRIBUTION/AVAILABILITY OF ABSTRACT UNCLASSIFIED/UNLIMITED ☐ SAME AS RPT ☒ DTIC USERS ☐	21 ABSTRACT SECURITY CLASSIFICATION **UNCLASSIFIED**
22a NAME OF RESPONSIBLE INDIVIDUAL	22b TELEPHONE NUMBER (Include Area Code) / 22c OFFICE SYMBOL

DD FORM 1473, JUN 86 **Previous editions are obsolete.**

UNCLASSIFIED

SECURITY CLASSIFICATION OF THIS PAGE

TABLE OF CONTENTS

LIST OF FIGURES

LIST OF FIGURES

1.0 INTRODUCTION

Organic coating provides one of the most cost-effective means for corrosion protection of structural alloys and is used extensively in both commercial and military applications. For many applications, corrosion protection by organic coatings and paints must not only protect against gross corrosive loss, but must maintain the dimensional integrity of the coated structure or part. For ship hulls, it is highly important to maintain smoothness which can be degraded by superficial corrosion or biofouling. Considerable progress has been made in the past several years toward gaining a general understanding of the mechanism of protection of metals by organic films. We now understand that the barrier nature of organic coatings plays a role in the corrosion protection by organic coatings, but adhesion and molecular blocking of active surface sites by the polymer under corrosive conditions determine for the most part good and poor coating behavior. An important objective of this program is to understand the role played by adhesion. In a recent review, Walter stated, "The concept of the paint film as an impermeable membrane has been largely discredited by permeability data for water and oxygen."[2] This reflects earlier speculation by Gerhart that, "in principle, a perfectly 'glued' surface coating can be reasoned as the ultimate protectant, provided, and if, the adhesion is perfect and enduring even allowing for absorbency and transport of nature's corrodents."[3] Previous efforts at the Science Center concluded that "...penetration of the coating by the environment by itself will not cause failure of the coated metal. However, loss of adhesion between the coating and the surface and cohesive failure of the coating brought about by the corrosion reaction provide the major driving forces for the propagation of failure."[1] Hence, the integrity of interfaces and interfacial zones under corrosive environments provides the focus for this proposed effort. The overall objective of this program is to develop new concepts for promoting the stability of polymer coating/metal systems based on observed fundamental molecular and mechanical mechanisms of degradation.

A number of material layers typically comprise a coating on a metal. These include: 1) a metal oxide or conversion product substrate formed as a result of surface preparation; 2) an interphase formed as a result of reaction of the organic primer with the substrate; 3) a corrosion-resistant primer; and 4) one or more top coatings. The top coating can serve a number of functions depending on the application. Since each layer

serves a different purpose, mismatches in physical and chemical properties will give rise to failure, particularly in adverse environments. Whereas the behavior of the top coating is beyond the scope of this project, the integrity of the metal/substrate, substrate/interphase and interphase/primer represents the focus of the proposed effort.

It is the objective of this project to understand the corrosion-induced degradation of adhesion of organic coating/metal systems in light of the previously described results which demonstrate that adhesion provides a critical barrier to corrosive failure. This understanding will lead to concepts for improving the resistance of the polymer/steel interface to degradation processes that occur under conditions of aqueous corrosion. This will be accomplished by understanding the detailed mechanism of environmentally induced adhesive and cohesive failure of the coating and the coating metal interphase. The program proceeds with three parallel tasks designed to:

1. Characterize the kinetics of failure at the organic coating/steel interface.

2. Examine the dynamics and structure of organic polymers on iron and steel surfaces.

3. Evaluate acid/base interaction of polymers on iron and steel surfaces occurring during the electrochemical reactions associated with corrosion.

In this reporting period, work primarily focused on Task 1. The new technique of acoustic microscopy has been applied in-situ to a coating undergoing potentiostatically controlled cathodic disbonding with the result that both the kinetics and microscopic structure of the disbond front has been characterized with detail not previously attained. The results show a formation of microblisters (possibly formed by an electro-osmotic mechanism) during the initial stages of cathodic disbonding of a polybutadiene coating in 0.5 M aerated NaCl. The tensile stresses which result from the formation of the microblisters contribute to the film rupture. This is a direct observation of the effect recently described on the basis of acoustic emission from a steel surface undergoing cathodic disbonding.[4]

2.0 ACOUSTIC MICROSCOPIC ANALYSIS OF CATHODIC DISBONDING OF POLYBUTADIENE

2.1 Background - Cathodic Disbonding

Corrosion of organic polymer-coated steel involves the initiation of anodic dissolution at a virtual pore or defect in the coating.[5,6] The anodic defect drives the adjacent region cathodic where oxygen reduction occurs to maintain the corrosion. The reduction of oxygen produces a locally alkaline environment which causes de-adhesion and disbonding, and therefore propagates the corrosive degradation of the coated steel. A number of proposed mechanisms for cathodic disbonding invoke chemical attack of the coating[7] or metal oxide,[8] attack of a metal/polymer interphase,[9] or alteration of the surface energy of the metal.[10] Two extensive reviews of the mechanism are available.[11,12]

Until now, no good nondestructive in-situ technique was available for following the disbonding while instantaneously measuring the rate. Although optical microscopic methods might be considered for monitoring the cathodic disbonding of polymer coatings, the sensitivity of acoustic microscopy to a disbond or weak bond as compared to optical microscopy makes it a superior method for detection of features at the disbond front, such as zones of polymer swelling, weak fluid boundaries and microblistering. Optical microscopy depends on refractive index mismatch between the fluid of the disbond and the polymer which is not great, whereas acoustic microscopy depends on the acoustical impedance mismatch between interfaces with and without weak bonds or disbonds. The contrast observed with scanning acoustic microscopy (SAM) is governed by the interaction of surface waves with the interface, and is therefore sensitive to the mechanical properties of solid/solid interfaces. Furthermore, differences in the velocity of sound in the coating polymer, as governed by water uptake and extent of crosslinking, may be expected under certain conditions to provide acoustic microscopic contrast. We would like to report preliminary results of the use of the acoustic microscope to make virtually instantaneous in-situ measurements of the rate and morphological details of cathodic disbonding of a hydroxy-terminated polybutadiene from carbon steel.

2.2 Experimental

2.2.1 Sample Preparation

A solution of four parts of hydroxy-terminated polybutadiene (PB-OH) (R-45HT, average MW = 2800, provided by the Sartomer Co.) in three parts mineral spirits containing 0.1% by weight vs solids of the active ingredients of Modiflow™ (Monsanto Co.) for leveling was spin-coated onto polished and degreased 7.6 cm x 7.6 cm and 0.055 cm thick steel Q-panels™. The coating solution was passed through a 0.2 μm Gelman alpha-200 Metricel™ membrane filter before coating to remove any dust or gel particles. The steel specimens were polished with 600 grit paper with distilled water, rinsed, dried and degreased at room temperature in hexane before applying the coating. Wet-coated samples were air-dried for 12 h and oxidatively crosslinked in an oven reaching 205°C for 9 min. The resulting coatings had a nominal 4 μm thickness. Individual specimens were prepared for polarization in the in-situ cell, each at a given cathodic potential. One specimen was polished with 1200 grit SiC followed by polishing in a kerosene medium using successively 15, 3 and 1 μm diamond paste. The resulting sample was then degreased and coated as for the other, more roughly polished specimens.

2.2.2 In-Situ Cell

Figure 1 shows a schematic of the in-situ cell and SAM lens. The Leitz Elsam system used for this work included a focused transducer which was typically operated at 1.0 GHz. The system also included an optical microscope which could be rotated into place to provide an optical image of the same field of view as the acoustic objective. A Pt ring counterelectrode, an Ag/AgCl reference electrode with a teflon salt bridge, the coated specimen as the working electrode sealed to the Delrin™ cell body using an o-ring seal, and a Delrin™ backplate comprised the in-situ cell. The electrolyte used for the tests was 0.5 M NaCl equilibrated with the laboratory environment. Using a SiC tool, two 2.5 cm scribes intersecting at right angles were placed in the coating before each test. For the 600 grit polished substrates, one line of the scribe was placed parallel and the other perpendicular to the 600 grit polishing marks. The sample was potentiostatically controlled using a PAR Model 173 potentiostat. Care had to be taken to maintain the proper electrolyte level (0.3 mm) in the cell so as not to contact the anodized aluminum of the acoustic lens heater/holder. As an additional precaution, the potentiostat

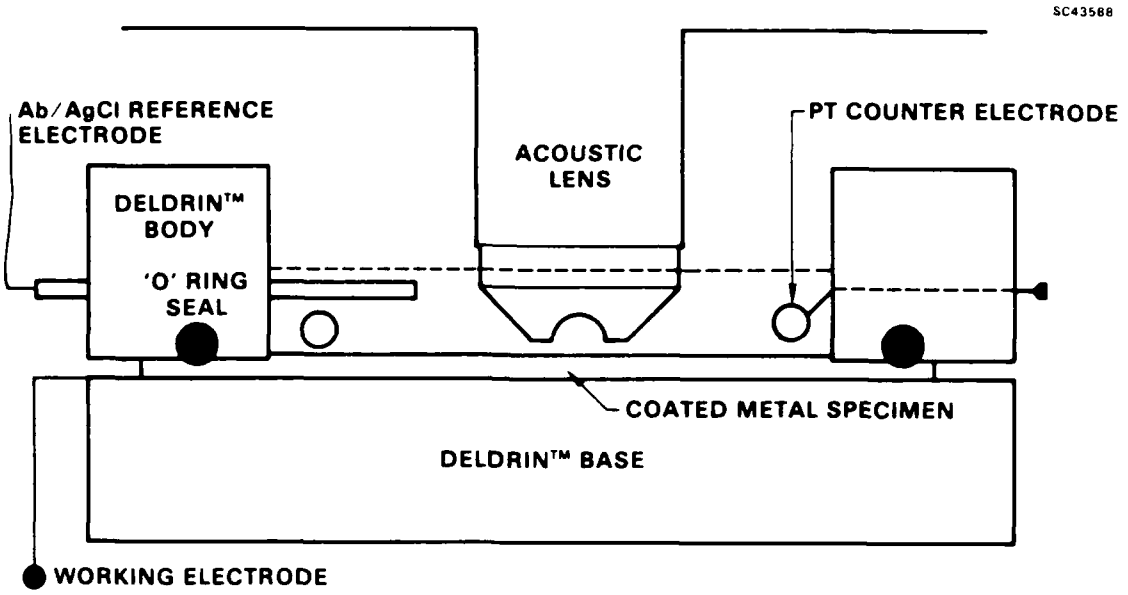

Fig. 1 Schematic of the in-situ cell.

was electrically isolated from the acoustic microscope. During each experiment, acoustic micrographs and the current were recorded at intervals ranging from 2 to 10 mins. The acoustic micrographs were typically taken adjacent to the scribe mark which was oriented parallel to the polishing marks for the 600 grit polished specimen.

2.3 Description of the Ultrasonic Detection Technique

To understand the ultrasonic method, consider the diagram in Fig. 2a. A buffer rod is depicted that has a piezoelectric transducer on one end and a concave lens on the other end. If the distance between the lens and the surface is equal to the focal length of the lens, then all of the rays incident on the surface will be reflected back into the lens and transmitted to the transducer in phase to produce a maximum response. The amplitude of this response will vary depending on the acoustic reflectivity of the specimen's surface. This reflectivity in turn is determined by the acoustic impedance of the specimen which is a function of its elastic stiffness and density. The contrast observed

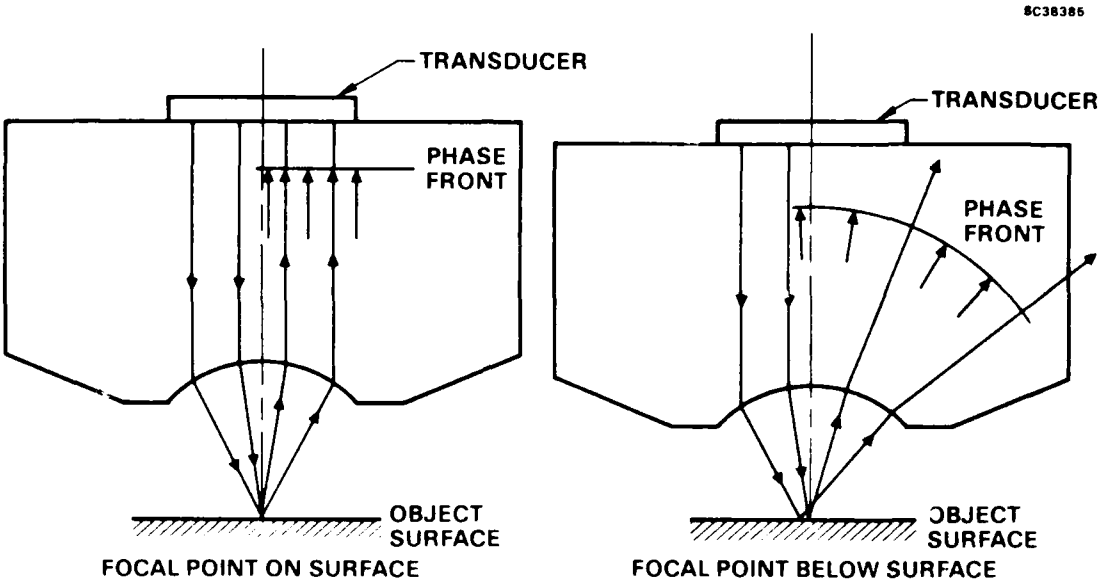

Fig. 2 (a) Buffer rod with piezoelectric transducer on one end and concave lens on the other. The lens is focused on the surface so that all reflected rays return to the transducer in phase; (b) when the separation between the lens and the surface is made less than the lens focal distance, most of the reflected rays are refracted away from the transducer. Only rays near the lens axis return to the transducer.

in an acoustic micrograph made under these conditions is analogous to the contrast observed in optical micrographs caused by changes in the dielectric constants of the material.

If the distance between the lens and the surface is decreased, as shown in Fig. 2b, most of the specularly reflected rays from the surface will be refracted by the lens so that they miss the transducer altogether. Only a small portion of the specularly reflected acoustic energy that is near the lens axis will be returned to the transducer. If there was no other effect, the output of the transducer as a function of the separation between the lens and the surface (z-distance) would decrease, as shown in Fig. 3. This is the pupil function of the lens. However, there is another effect, as illustrated in Fig. 4. For sufficiently large numerical aperture lenses, there is a ray incident on the surface at the proper angle (designated θ_R) to generate a surface acoustic wave (SAW). This wave propagates along the surface and reradiates energy back into the water at an angle that

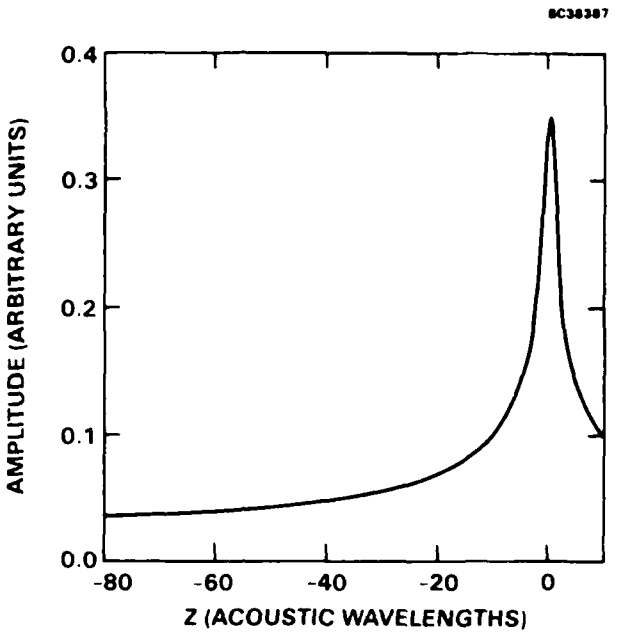

Fig. 3 Pupil function of the lens in the absence of SAWs illustrating how the electrical signal from the transducer varies with the separation of the lens and the surface.

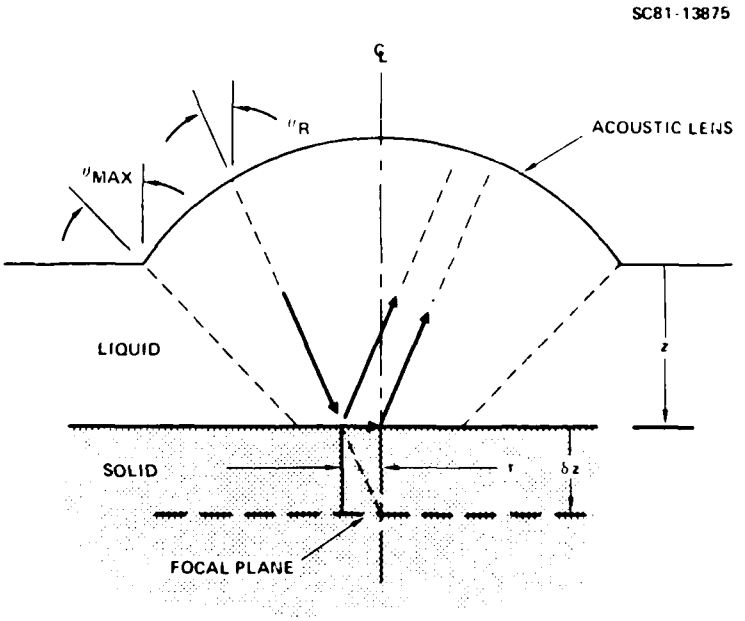

Fig. 4 Schematic of the acoustic lens illustrating the generation of a SAW by rays incident on the surface at the appropriate angle (θ_R). The SAW propagates along the surface as it reradiates energy back into the water. Some of this energy enters the lens at the correct distance from the lens axis to be refracted parallel to the lens axis and returns to the transducer.

is equal to θ_R. If the lens is closer to the surface than its focal length, the SAW will propagate a short distance before the reradiated wave will enter the lens at the proper distance from the lens axis to be refracted parallel to the lens axis and be received by the transducer. The propagation distance is a function of z and causes a variable phase difference between this wave and the wave that is specularly reflected from the surface (Fig. 2b). This leads to alternative constructive and destructive interference between the two groups of waves. When the output of the transducer is plotted vs z, there is a ripple pattern superimposed on the pupil function of the lens, as shown in Fig. 5. The period of the ripple depends on the SAW velocity.

The ripple pattern and the contrast changes associated with it has come to be known as the V(z) effect. To understand how the contrast in an image changes due to changes in the SAW velocity, consider the example illustrated in Fig. 6, in which the surface has two distinct regions (A and B) that have different SAW velocities. Assume the lens is positioned at a distance z_o from the surface. The V(z) curves for the two regions, labeled A and B, are shown in Fig. 6. When the lens is over region A, the output is V_A.

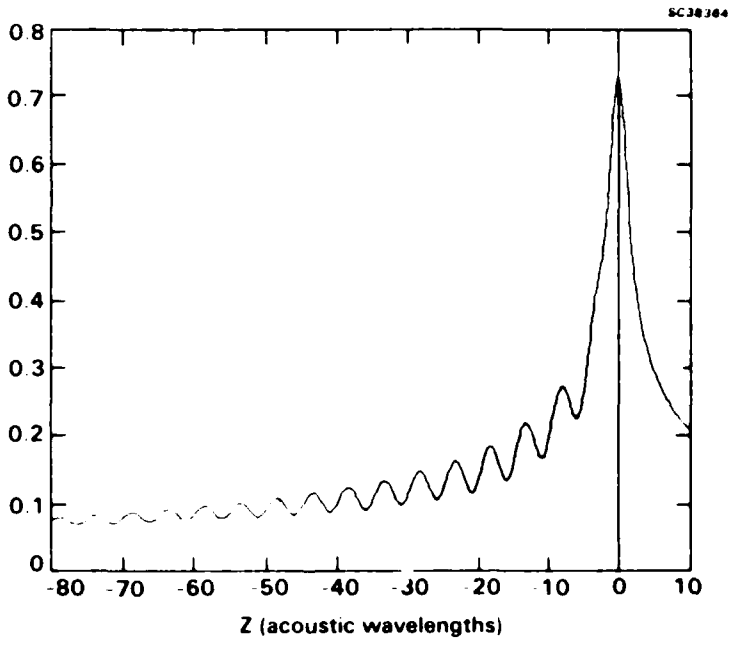

Fig. 5 Pupil function of the lens in the presence of SAWs illustrating the ripple pattern arising from the alternating constructive and destructive interference between the specularly reflected energy and the reradiated energy from the SAW.

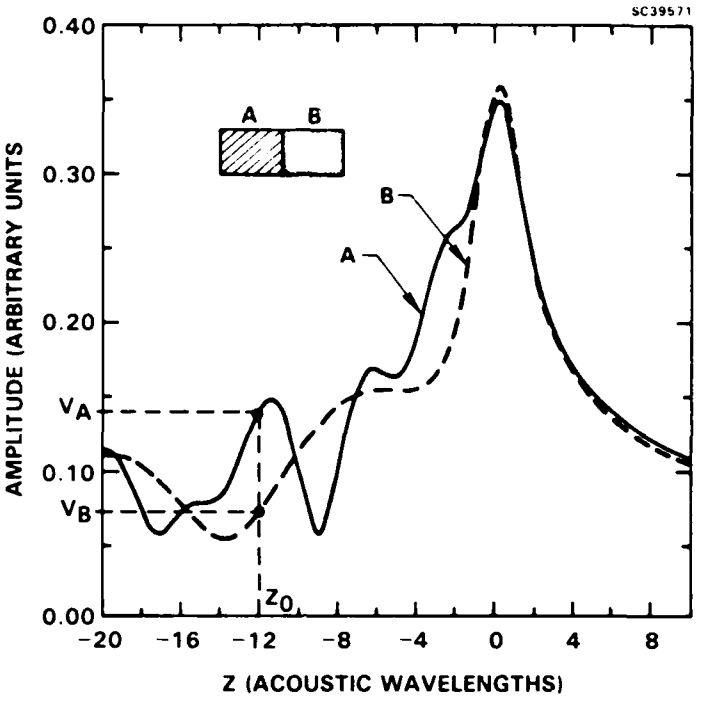

Fig. 6 The insert shows a surface with two regions, A and B, that have different SAW velocities. The curve labeled A is characteristic of region A of the sample. The curve labeled B is characteristic of region B. The change in the transducer output voltage obtained from the two curves produces a change of contrast in the image as the lens is scanned over the sample.

When the lens is over region B, the output is changed to V_B. For this particular lens to surface, separation distance V_A is the largest signal, but for other separation distances, V_B could be the largest. Thus, it is possible to obtain contrast reversal in an image by slightly changing the focus of the lens. The effect is also sensitive to changes in topology of the sample. If a third region, C, has the same SAW velocity as region A but is higher than region A, the output signal will change, as illustrated in Fig. 7.

A disbonded film will be detected because the SAW velocity will change significantly in the region of the disbond. The disbonded film may also lift up. It will then be detected because of the change in height.

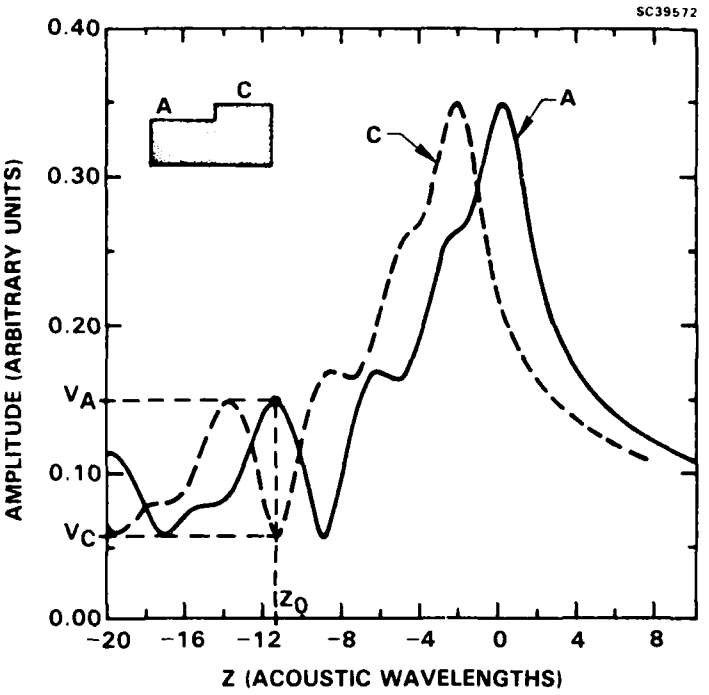

Fig. 7 The insert shows a surface with a step in height between region A and C. The operating point on the V(z) curve changes to produce a change in the transducer output voltage. This results in a change of contrast in the image as the lens are scanned over the sample. As the lens to surface separation changes, the contrast of the two regions can reverse.

2.4 Results of Acoustic Microscopic Analysis of Cathodic Disbonding of Polybutadiene on Steel

Figure 8 shows acoustic micrographs for a PB-OH coated steel specimen polarized at -850 mV vs Ag/AgCl. The focus is at the metal coating interface. The polishing scratches are clearly visible as well as 5-150 μm defects apparently in the coating. The grains of the substrate are just barely visible in the micrograph taken at 1.5 min (Fig. 8). After several minutes of polarization, the disbond front appears as a collection of 10-50 μm apparent microblisters which nucleate and grow with time. The fact that the apparent microblisters are three-dimensional can be seen by the onset of interference rings observed after 100 min exposure (Fig. 8) caused by the upward expansion of the blister (see Appendix, Section 5.0). Theoretical calculations show that the change in height represented by one fringe equals one-half of an acoustic wavelength for the medium contained within the blister. Note that the acoustic wavelength at 1 GHz in

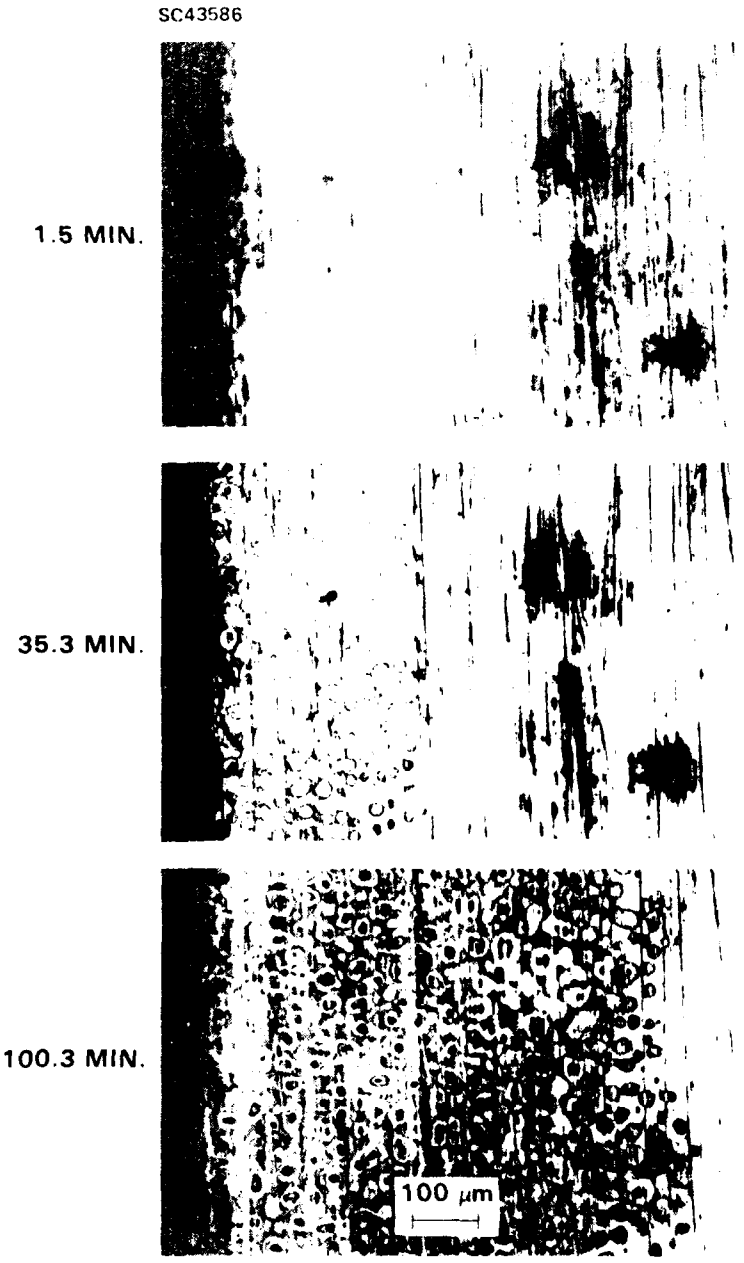

Fig. 8 Acoustic micrographs for a hydroxy-terminated polybutadiene coated steel specimen polarized in 0.5 M NaCl at -850 mV vs Ag/AgCl for 1.5, 35.3 and 100.3 min.

water is 2.5 μm and about 1.6-1.8 μm for polymers. Previous work in this laboratory allowed an estimate of 1.6 μm at 1 GHz for the wavelength of sound in an epoxy polyamide.[1] The heights of the blisters in Fig. 8 are then 1.5-3 μm, assuming wavelengths between 1.5-2.0 μm. The morphology of the nucleation and growth of the array of microblisters characterizing the disbond is essentially the same regardless of the potential between -1100 mV and -700 mV vs Ag/AgCl. The microblisters may either be pockets of electroosmotically formed electrolyte or swollen regions of the heterogeneous polymer.

A time series of micrographs allowed a virtually instantaneous determination of the extent of disbonding defined by the microblister front and hence the rate of disbonding. Figure 9 shows plots of the distance of the disbond from the scribe mark, d, as a function of the square root of time in minutes, $t^{1/2}$ for different conditions of polarization. After an initial induction time, t_o, it was found that the disbond front defined by the presence of microblisters moves at a rate which is proportional to $t^{1/2}$. The data could not be fit as well to a linear function of time, since a significant decrease in rate

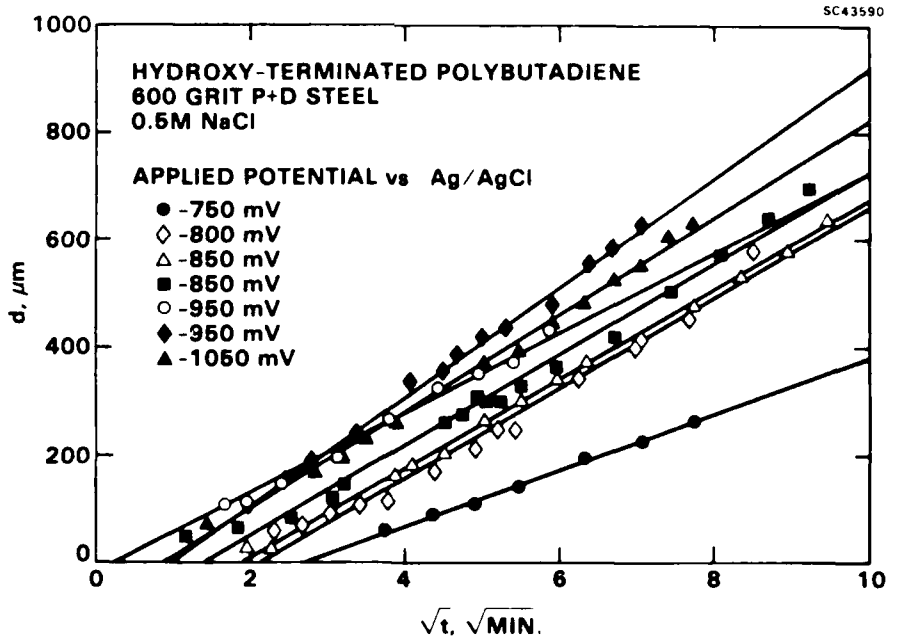

Fig. 9 The distance of the disbond from the scribe mark, d, as a function of the square root of time in minutes for scribed specimens polarized at indicated potentials vs Ag/AgCl.

occurred with time. Hence, the $t^{1/2}$ behavior was determined to be statistically consistent with the data. This behavior is consistent with the model proposed by Thornton[12] and the observations of Leidheiser and Wang.[10] Leidheiser and Wang show a linear dependence of the area of a circularly symmetric region with time ($t^{1/2}$ dependence of the radius). The rate constant, K_d, expressed as $\mu m/min^{0.5}$ increases with decreasing (more cathodic) potential. K_d varies more slowly with potential below -900 mV and remains potential-independent down to -1100 mV where hydrogen evolution commences (Fig. 10). The initiation time, t_o, decreases with decreasing potential over the same potential region becoming constant for potentials below -950 mV (Fig. 11).

One test was performed with a polarization of -750 mV on a coated, polished and degreased steel specimen that had been polished to a 1 μm finish before spinning on and curing of the hydroxy-terminated polybutadiene coating. The initiation time for the onset of disbonding for this specimen remained nearly identical to that for specimens polished with 600 grit SiC paper, giving a t_o of 7.4 min (Fig. 11). However, the rate con-

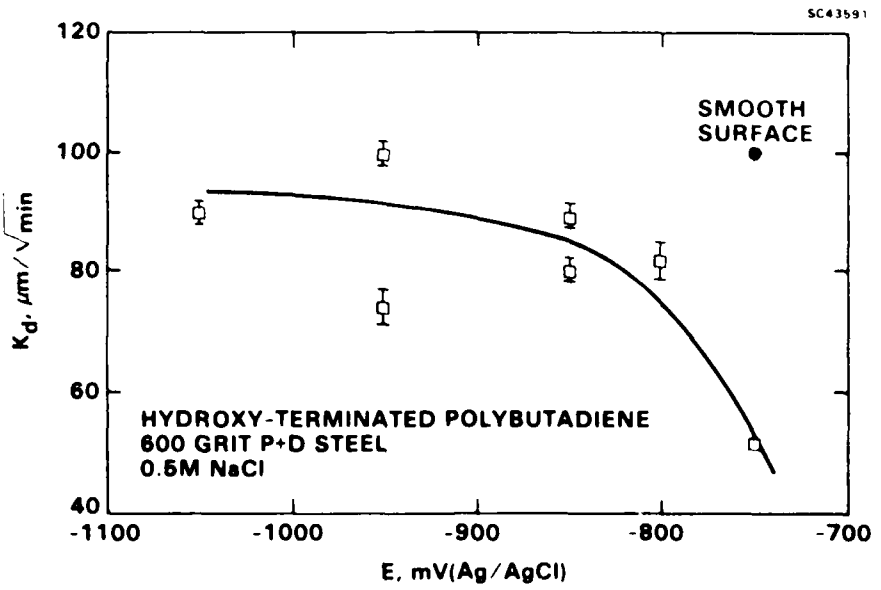

Fig. 10 Disbond rate constant, K_d, as a function of potential in mV vs Ag/AgCl.

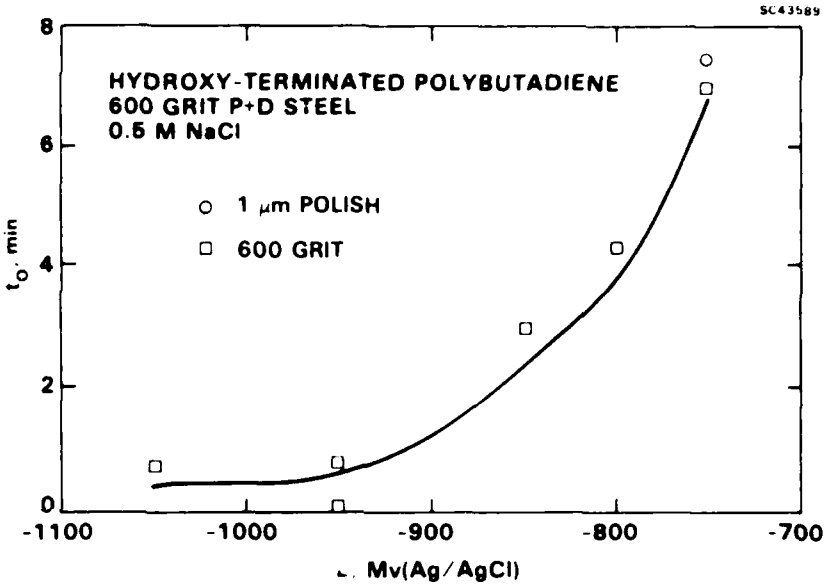

Fig. 11 Initiation time, t_o, as a function of potential (Ag/AgCl).

stant, K_d, for propagation of the disbond for the 1 μm finished specimens was significantly greater than that of the sample polished with 600 grit SiC, giving a value of 104 μm/(min)$^{1/2}$ as compared to 52 μm/(min)$^{1/2}$ for the 600 grit polished specimen. This result agrees with the explanation made elsewhere[14] that a disbonding rate depends on the true surface area of the bond. Since more surface bonds must be broken for a rough surface to obtain the same extent of superficial disbond length as compared to a smooth surface, the apparent disbonding rate for a rough surface appears to occur at a slower rate.

After completing a test, the electrolyte was removed and scotch tape applied to the polymer and pulled to remove the disbonded region. The region mechanically removed by the tape was about 50 μm ahead of the last acoustic microscopic observation of blisters. At first, this was attributed entirely to a weak bond ahead of the blisters. However, in subsequent tests, it was observed that there was an apparent delay of several minutes after the removal of the potential before the movement of the disbond front completely stopped. This is illustrated in Fig. 12. At about 95 min, the current is removed. However, the disbond front appears to move another 50-100 μm before stopping at 10 min after removal of the current (Fig. 12).

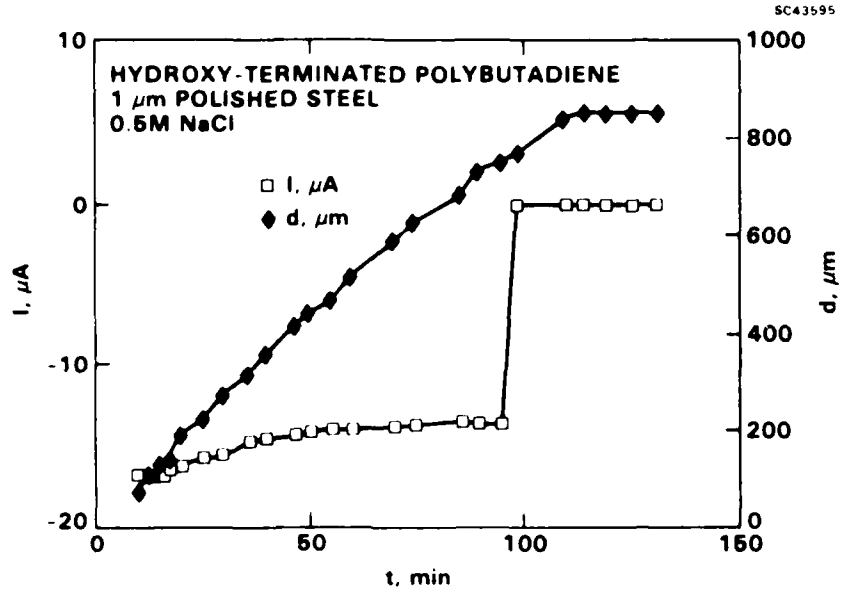

Fig. 12 Current and disbond distance as a function of time for the 1 μm polished steel.

During each disbonding test, the current was monitored and observed with time as follows:

$$i = i_o + K_i t^{1/2} \quad .$$

At potentials more positive than -900 mV vs Ag/AgCl, the magnitude of the cathodic current decreases with time (K_i is positive), but for potentials more negative than -950 MV, the magnitude of the cathodic current increases with time (K_i is negative), as shown in Fig. 13. Most of this current flows at the scribe end, therefore cannot be considered as indicative of the electrode kinetics of the interface. One must also consider the possibility that there is sufficient IR drop down the disbond such that the potentials are valid for the scribe mark, but not the disbond front. The potential of -950 mV vs Ag/AgCl represents the potential where the reaction that occurs at the scribe mark becomes determined by the activation-limited hydrogen evolution rather than the diffusion-limited oxygen reduction. The diffusion-limited rate for oxygen reduction at potentials

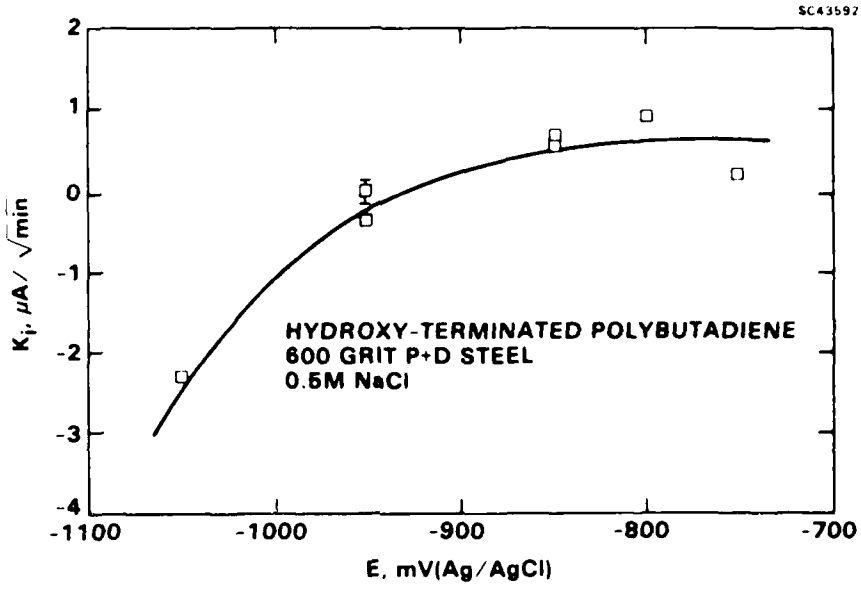

Fig. 13 Rate constant, K_i, for the time dependence of the current plotted as a function of applied potential.

more anodic (positive) than -950 mV is independent of potential, as shown by the absence of change in the current with respect to potential at potentials more positive than -950 mV (Fig. 14).

To get a less cluttered image of the processes occurring at the disbond front, the propagation of a disbond occurring at an applied potential of -750 mV on the steel specimen that was polished to a 1 μm finish was examined. The smooth surface allowed examination of the cathodic disbonding process in more detail than for the 600 grit surfaces. Figure 15 shows an acoustic micrograph of the specimen obtained after the disbond had propagated for 39 min in the 0.5 M NaCl solution. A very faint line 38 μm ahead of the microblisters can be seen (see arrow in Fig. 15). After 95 min, the polarization was turned off. After a delay of 4 min, a well-defined boundary line was observed which remained unchanged for 25 min with the exception that several microblisters formed ahead of this line (Fig. 16).

To evaluate the reversibility of the disbonding process, several specimens were cathodically treated at -1050 mV for 1 h and subsequently removed from the electrolyte and equilibrated with the laboratory atmosphere for several hours. Upon applying scotch

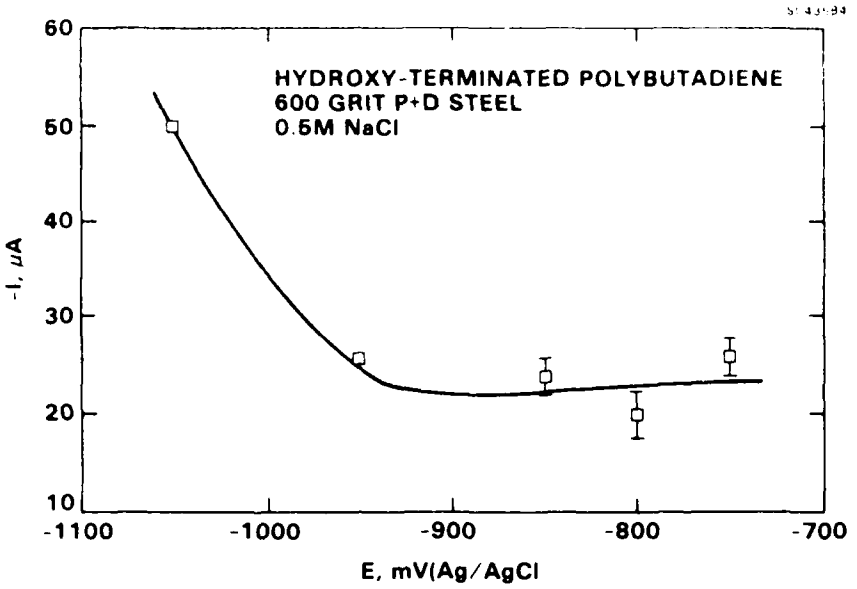

Fig. 14 Average current at the scribe as a function of applied potential vs Ag/AgCl.

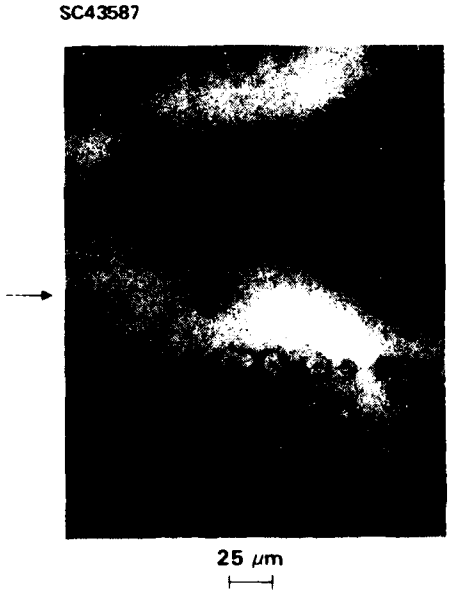

Fig. 15 Acoustic micrograph of the disbond front for the 1 μm polished specimen after being polarized at -750 mV vs Ag/AgCl for 39 min.

Fig. 16 Acoustic micrograph of the disbond front for the 1 μm polished specimen 25 min after removing the -750 mV polarization. Open-circuit potential is -526 mV (Ag/AgCl).

Fig. 17 Montage of acoustic micrographs of a specimen that has been cathodically disbonded at -1050 mV and then allowed to dry.

tape to the region around the scribe, no pulloff of the coating was observed; the disbond zone had at least partially rehealed. However, some microblisters remained (Fig. 17) at the disbond front surrounding the scribe and around defects in the coating at the right side of the figure. These blisters could not be removed even by holding the specimen for 12 h in a 5 mTorr vacuum dessicator. These microblisters were not voids, since the acoustic response gave the familiar ring pattern (see Appendix) as opposed to a black spot expected for a microvoid. Hence, the microblisters remaining after the 'dry-out' either irreversibly contained fluid or were composed of swollen polymer.

2.5 Discussion of Results of Acoustic Microscopy

These results are consistent with the following steps in the cathodic disbonding process:

1. Diffusion of water and oxygen into a region of coating/metal oxide interphase.

2. Dissolution of oxide/polymer interphase to form an occluded nucleation site for enhanced oxygen reduction and OH^- concentration.

3. Electroosmotic transport of water into the interphase to dilute the NaOH, thereby providing the pressure to deform the coating to form the microblisters and enhance the growth of the disbond. The aggressive alkaline environment in the microblisters and the pressure in the blister drives further attack of the interphase to propagate the failure.

Castle and Watts have previously shown that an iron oxide/polymer interphase exists between the bulk polymer and the metal oxide substrate for this particular coating system.[9] The diffusion of water into the interphase region at the leading edge of the disbond is consistent with the observation of a $t^{1/2}$ time dependence (Fig. 9) and the detection of a narrow front (weak fluid boundary layer) ahead of the microblisters as observed on the highly polished specimen (Figs. 15 and 16). The $t^{1/2}$ time dependence is predicted by the model described by Thornton and coworkers.[13] The presence of OH^- at the interface or interphase region as described by Castle and Watts[9] enhances the absorption of

water at a weak fluid boundary layer. Continued electrochemical reactions reduce oxygen to form OH^- whose charge is balanced by the influx of hydrated Na^+. Charge transport by the hydrated cation diffusion to the interphase provides the mechanical pressure due to osmosis for forming the observed microblisters. The mechanical force due to the osmotic pressure ultimately drives the disbond along the weakened interface. The existence of three-dimensional microblisters demonstrates the existence of an environmentally enhanced mechanical force similar to and ultimately having the same effect as swelling of the polymer, but perhaps it is not identical to the commonly considered mechanisms of swelling, as suggested elsewhere.[13] Nevertheless, the mechanical stresses induced by the electroosmotic formation of the microblisters will exceed the peel or shear strength of the already weakened bond ahead of the sodium hydroxide filled microblisters.

While the presence of high pH regions at the coating/metal interface may ultimately lead to the dissolution of the metal oxide, particularly under reducing conditions as shown by Ritter,[8] or may produce alkaline attack on the polar groups of the polymer as demonstrated by others,[6] it is not clear that these are necessary conditions of cathodic disbonding, but rather results of attack of the freshly exposed interfaces produced after the actual rupture induced by the electroosmotic swelling of the coating at the interface as observed here.

3.0 SUMMARY OF RESULTS

An in-situ cell has been devised for allowing examination of coated metal by SAM. The in-situ acoustic microscopic method provides a rapid nondestructive method for determining the rate of disbonding of organic coatings. Cathodic disbonding for a number of hydroxy-terminated polybutadiene coated specimens has been examined as a function of potential. The results show that potentials more negative than -550 mV vs Ag/AgCl accelerate cathodic disbonding. Furthermore, cathodic disbonding proceeds by the formation of a weak fluid boundary layer just ahead of a region of electroosmotically formed microblisters. The build-up of NaOH in the microblister promotes water entry and attack of the interphase composed of metal oxide and polymer between the coating and the oxide substrate, while the osmotic pressure in the microblisters provides the mechanical force necessary to produce the rupture in the interphase zone.

4.0 FUTURE PLANS

The examination of cathodic disbonding kinetics for the hydroxy-terminated polybutadiene will continue for increasing (more anodic) potentials to establish the electrochemical conditions where the reaction ceases. The method will be applied to rapidly determine the disbonding rate constant, K_d, for combinations of polymers (including epoxy polyamide coatings) and surface treatments (including phosphating and application of adhesion promoters). The disbonding mechanism on Au substrates where no significant oxide forms will be examined to establish the relative importance of metal oxide dissolution/reduction. The method will also be extended to thicker coatings which have a more practical importance. Additional work will be performed on coated, highly polished substrates to obtain better resolved micrographs of the weak fluid boundary layer ahead of the nucleating microblisters.

The approach for the second task aimed at evaluating the structure and reactions of the polymer metal interphase entails the use of an in-situ electrochemical cell[16] to condition steel containing thin films of polymer in the vacuum chamber of an XPS and AES spectrometer. The first phase of this work will take place in a 1.0 M NaOH solution which simulates the solution at the locus of the cathodic failure zone. Some modification of the existing cell was necessary to accommodate the NaOH solution and nears completion. The relevant potentials where the oxide or oxide/coating interphase degrades as well as the organic functionality involved in promoting adhesion will be determined.

5.0 APPENDIX - THEORETICAL ANALYSIS OF SAM RESPONSE TO A POLYBUTADIENE FILM ON STEEL

The calculations of the response of the SAM to a polybutadiene film on a steel substrate are based on a simple model consisting of water covering a polybutadiene film on a semi-infinite steel substrate (Fig. A.1). Other films can be added between the polybutadiene film and the substrate to simulate a disbond. The films are assumed to be lossless. Further, the films must be solids in the sense that they have a nonzero value for the shear elastic constant (the C_{44} element of the elastic tensor). To simulate the disbond filled with liquid, C_{44} is made very small compared to C_{11}. We assume that the error introduced by this approximation can be neglected. Finally, the waves that impinge on the layered model from a source in the water are assumed to be continuous.

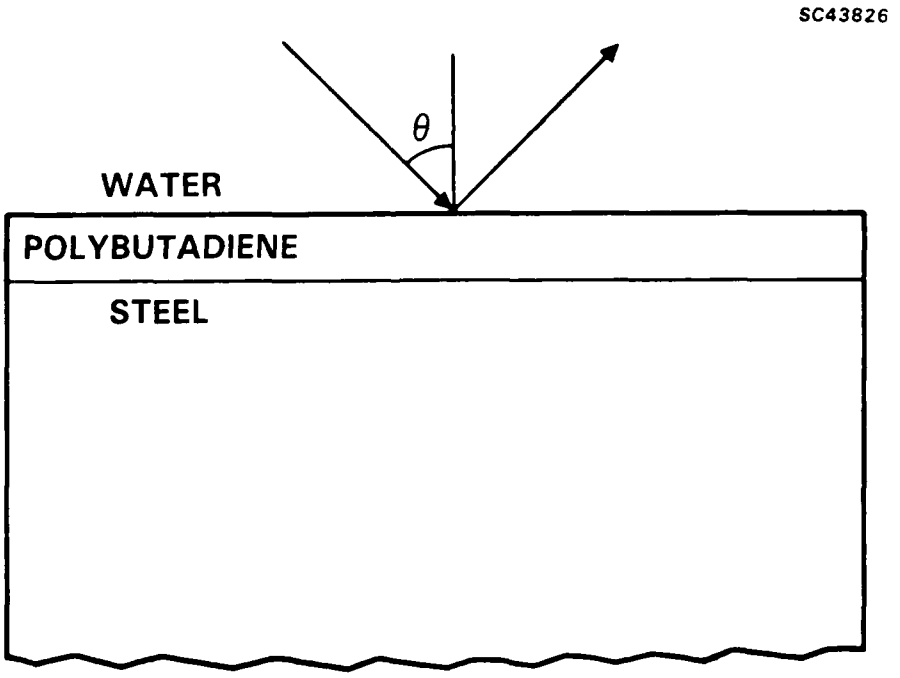

Fig. A.1 Model for the calculations of the complex reflection coefficient of a polybutadiene film on a steel substrate.

First, the complex reflection coefficient of a longitudinal acoustic wave incident at an angle θ is calculated for a range of angles corresponding to the numerical aperture of the acoustic lens (θ_{max} = 50° for the lens used in the experiments). This calculation solves the acoustic Fresnel equationg using techniques described by Brekhovskikh[17] and Bray.[18] Next, the voltage response of the transducer is calculated for a particular separation of the lens and the film. The distance is designated z and is measured from the lens focal point to the surface of the film. The expression for the voltage is given by the integral in Eq. (A1).[19,20]

$$V(z) = \int_{\theta=0}^{\theta_{max}} P(\theta)^2 \, R(\theta) \, e^{i2kz\cos(\theta)} \sin\theta \cos\theta \, d\theta \qquad (A1)$$

where $P(\theta)$ is the pupil function of the lens. For the purpose of these calculations, it is assumed to have the simple form:

$$P(\theta) = \cos\left(\frac{\pi}{4} \cdot \frac{\theta}{\theta_{max}}\right) \qquad (A2)$$

$R(\theta)$ is the complex reflection coefficient. Note that the positive z direction is measured outward from the focal point.

When this calculation is made for a 4 μm polybutadiene film on steel, the result shown in Fig. A.2 is obtained. Note that there are two dominant peaks. One occurs when the focus of the lens is near the surface of the film (z = 0) and the other occurs when the focus is 8.4 μm below the surface of the film. This should not be thought of as focusing below the surface, but as altering the relative phases of the waves that are reflected from the surface and recombined at the transducer.

The highest contrast images of the disbonded region are obtained when the focus is near or at the second peak. The microblisters observed in the disbond region give rise to interference fringes caused by the local change in height of the film. A calculation of the change in the transducer voltage as the thickness of an intermediate layer increases produces the cyclic result shown in Fig. A.3. Note that the variation of the voltage at a z distance corresponding to the second peak is greater than that for z = 0. Thus, the contrast observed in the micrograph will be higher for this focal position. Also note that the period of the variation is $\lambda/2$, where λ is the longitudinal acoustic wavelength measured in the disbond layer. Thus, the height of the microblisters can be measured in absolute units if desired.

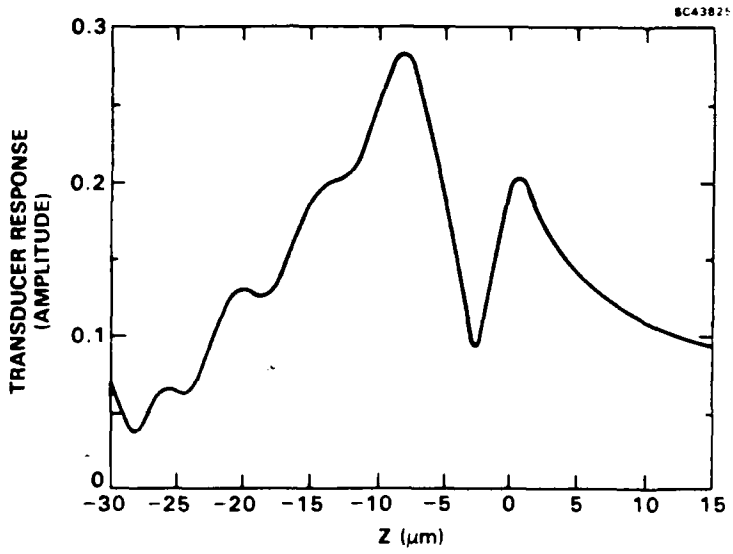

Fig. A.2 Calculated V(z) curve for 4 μm polybutadiene film on steel.

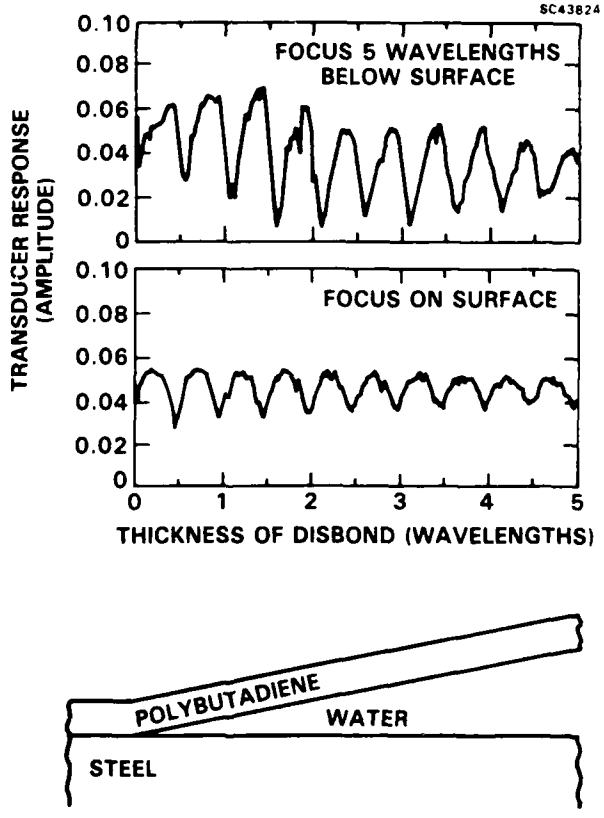

Fig. A.3 Calculated change in the transducer voltage, V, vs the thickness of a water layer simulating a disbond between the polybutadiene film and the steel substrate. Results are shown for two values of the z distance between the lens focal point and the film surface.

6.0 REFERENCES

1. F. Mansfeld and M. Kendig, "Lifetime Prediction of Organic Coating/Metal Systems," Final Report for the period July 1, 1979 - October 31, 1985, Contract No. N00014-79-C-0437, Science Center Report No. SC5222.FR (1986).
2. G. Walter, Corr. Sci. 26 (1), 27 (1986).
3. H. Gerhart, "Prophetic Imperatives in Corrosion Control," in Corrosion Control by Coatings, H. Leidheiser, Jr., ed., Science Press (1979).
4. T. Tsura, A. Sagara and S. Haruyama, Corrosion 43 (11), 646 (1987).
5. M. Kendig and H. Leidheiser, J. Electrochem. Soc. 123 (7), 982 (1976).
6. F. Mansfeld and M. Kendig, "Electrochemical Impedance Tests for Protective Coatings," ASTM Special Testing Publication, No. 866, 1985.
7. J.S. Hammond, J.W. Holubka, J.G. DeVries and R.A. Dickie, Corr. Sci. 21 (3), 239 (1981).
8. J. Ritter, J. Coating Technology 54, 695 (1982).
9. J.E. Castle and J.F. Watts, I&EC Products Res. and Dev. 24, 361 (1985).
10. E. Koehler, Corrosion 40, 5 (1984).
11. H. Leidheiser, Jr., W. Wang and L. Igetoft, Prog. in Inorg. Coatings 11, 19-40 (1983).
12. H. Leidheiser, Jr., J. Adhes. Sci. Tech. 1 (1), 79 (1987).
13. J.S. Thornton, R.E. Montgomery and J.F. Cartier, "Failure Rate Model for Cathodic Delamination of Protective Coatings," NRL Memorandum Report 5584, 1985.
14. X.H. Jin, K.C. Tsay, A. Elbasir and J.D. Scantlebury, "The Adhesion and Disbonding of Chlorinated Rubber on Mild Steel," in Proc. of Symp. Corrosion Protection by Organic Coatings, M.W. Kendig and H. Leidheiser, Jr., eds., Electrochem. Soc., 87-2, 1987.
15. S. Haruyama, M. Asari and T. Tsuru, "Mass Transport in Blistering of Coated Steel," in Proc. of Symp. Corrosion Protection by Organic Coatings, M.W. Kendig and H. Leidheiser, Jr., eds., Electrochem. Soc., p. 11.
16. J. Lumsden and P.J. Stocker, J. Electrochem. Soc., to be published.

17. L.M. Brekhovskikh, Waves in Layered Media, Academic Press, NY (1960).
18. R.C. Bray, "Acoustic and Photoacoustic Microscopy," Ph.D. Thesis, Stanford University, 1981.
19. C. Ilett, M.G. Somekh and G.A.D. Briggs, "Acoustic Microcsopy of Elastic Discontinuities," Proc. R. Soc. Lond. A393, 171-183 (1984).
20. C.J.R. Sheppard and T. Wilson, Appl. Phys. Lett. 38, 858-859 (1981).

END

DATE

FILMED

6-88

DTIC